Struct Multidisc Optim (2010) 40:257–269
DOI 10.1007/s00158-009-0358-4

RESEARCH PAPER

Multi-objective optimization of free-form grid structures

P. Winslow · S. Pellegrino · S. B. Sharma

Received: 20 October 2008 / Revised: 22 December 2008 / Accepted: 7 January 2009 / Published online: 7 February 2009

Abstract Computational modeling software facilitates the creation of any surface geometry imaginable, but it is not always obvious how to create an efficient grid shell structure on a complex surface. This paper presents a design tool for synthesis of optimal grid structures, using a Multi-Objective Genetic Algorithm to vary rod directions over the surface in response to two or more load cases. A process of grid homogenization allows the tool to be rapidly applied to any grid structure consisting of a repeating unit cell, including quadrilateral, triangular and double layer grids. Two case studies are presented to illustrate the successful execution of the optimization procedure.

Keywords Structural optimization · Multiobjective · Grid shell · Free form structure · Homogenisation

1 Introduction

The advent of free-form 3-D modeling software has allowed architects and designers to create any shape imaginable. In order to physically realize these computer models, say as a building or a sculpture, an internal armature can be used along with non-load bearing panels to create the required external surface e.g. Gehry's Guggenheim Museum in Bilbao. Use of a 'grid-shell' structure, consisting of a lattice of rods (see Fig. 1) may be more desirable due to the potential for reductions in material usage and increased internal space. However, it is not always obvious how to create an efficient grid structure on a given surface.

The need for new computational structural engineering tools that can be applied to complex geometries has been highlighted by several authors, including Schlaich et al. (2005). Michalatos and Kaijima (2007) describe a number of new tools for grid mapping. In general, the task of creating an efficient grid structure is made more difficult by the diverse range of requirements on architectural engineering projects, which might include: ultimate limit failure criteria, serviceability/comfort criteria for a variety of load cases, and aesthetics. As such, a conventional optimization algorithm which finds a single 'best' structure may not be desirable since it can restrict overall design freedom. Therefore this paper will present a novel method for synthesis of grid structures on free-form surfaces, which utilizes a Multi-Objective Genetic Algorithm (MOGA) to find optimal rod orientations.

Topology optimization can be used to create an efficient structure on a given surface, as described by Maute and Ramm (1997). However, the solutions obtained are akin to a continuum shell with holes cut away, and so complex post-optimization rationalization would be required to convert this into a structure consisting of discrete rods and nodes.

P. Winslow (✉)
Engineering Department, Cambridge University,
Trumpington Street, Cambridge CB2 1PZ, UK
e-mail: pjw63@cam.ac.uk

S. Pellegrino
California Institute of Technology,
Pasadena, CA 91125, USA
e-mail: sergiop@caltech.edu

S. B. Sharma
Buro Happold, Camden Mill, Lower Bristol Road,
Bath BA2 3DQ, UK
e-mail: Shrikant.Sharma@BuroHappold.com

Fig. 1 British Museum Great Court Roof, London, UK (Courtesy of Andrew Dunn)

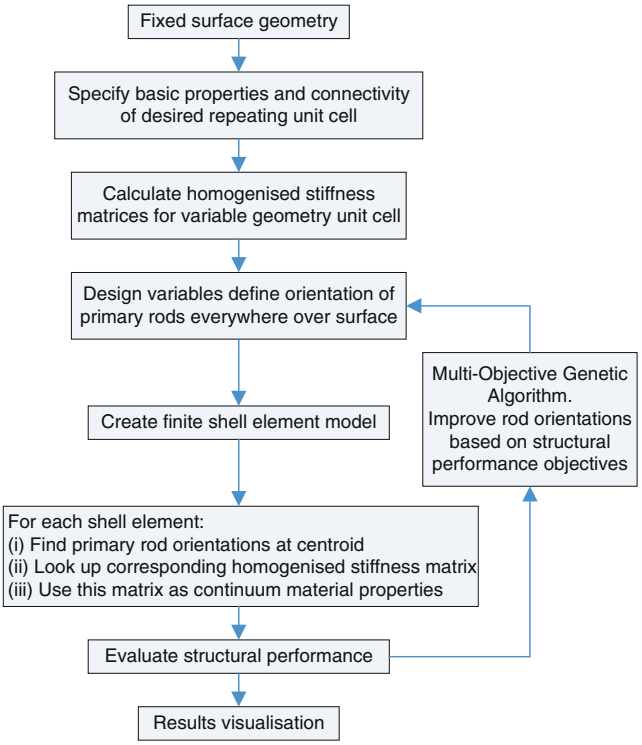

Fig. 2 Overview of methodology

Prager and Rozvany, e.g. (1979, 1982), develop simple analytical solutions for optimal 'grid-shells' (also referred to as 'arch-grids') of minimum weight. Variations in orientation of rods are considered, as well as variations in height; hence the surface geometry is not necessarily fixed. This may be useful to inform the design engineer of the best structural scheme for a given set of boundary conditions. However, there is a practical requirement in many architectural projects to realize a given, fixed, surface form.

The algorithms developed in this paper are based on techniques for finding optimal orientation of fibres in a composite, e.g. Gurdal and Olmedo (1993), which allows the practical limitations of topology optimization and analytical solutions to be avoided. Although the final structure must be a set of discrete rods, a process of homogenization allows for the lattice of rods to be represented by anisotropic continuum shell finite elements throughout the optimization process. A novel parametrization of the problem reduces the number of design variables, thus making the use of a MOGA more feasible and improving the constructibility and visual appeal of optimized designs. The basis of this approach was first described by the authors (Winslow et al. 2007), but this current paper describes significant new developments to the method and explores the use of a MOGA in detail.

2 Overview of methodology

Figure 2 gives an outline of our new optimisation technique. The starting point is a surface geometry which remains fixed throughout the whole procedure. On this surface we wish to create an optimal grid shell by varying the orientation of two primary sets of rods. The designer specifies a primary rod spacing, L, defines rod cross sections and whether triangulation and/or infill panels are required. These choices define the basic connectivity and properties of the grid's repeating unit cell. However, the precise unit cell geometry will vary as primary rod directions change, see Fig. 3.

Before starting the optimisation process, the homogenised stiffness matrix is calculated for all possible unit cell geometries. The result is that the components of the homogenised stiffness matrix are defined as functions of the angle between the two primary rods. See Section 3 for full details.

The next step is to use a modest number of design parameters to define directions of the two primary sets of rods on the surface, as described by the scheme in Section 4. A larger number of parameters will allow creation of more complex rod paths and thus a wider range of grid geometries, but at the expense of convergence rate.

The surface is meshed with shell finite elements, and at the centroid of each element the two primary rod orientations are computed (Figs. 9 and 10). Calculation of the angle between the primary rods allows the appropriate homogenised stiffness matrix to be rapidly looked up, and input as unique (anisotropic)

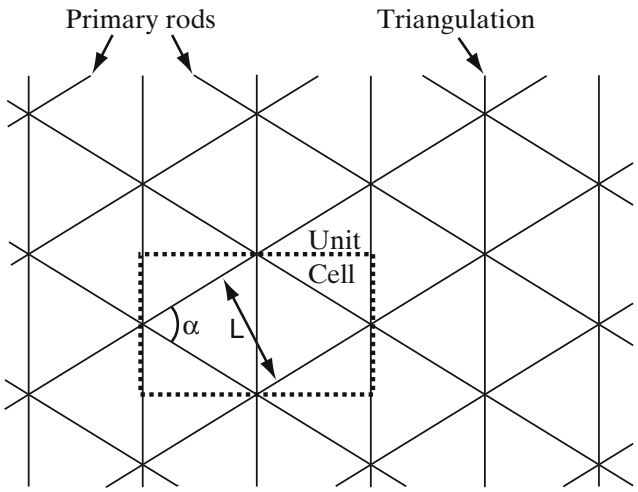

(a) Regular triangulated grid

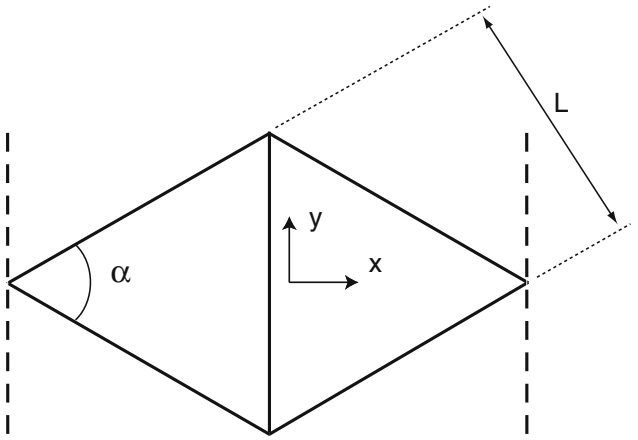

Solid lines define rods with I_{xx}, I_{yy}, J, A
Dashed lines define rods with $I_{xx}/2$, $I_{yy}/2$,$J/2$

(b) Unit cell

Fig. 3 Definition of repeating unit cell for a triangulated grid of rods (**a**, **b**)

material properties for that particular continuum shell element. Note that the average direction of the primary rods defines the orientation of this equivalent stiffness anisotropic material. Since the rod orientations are able to vary over the surface, so each shell element can have different continuum material stiffness properties. Suitable load cases are then applied to the FE model and the structural performance is evaluated.

Using structural performance as the objective(s), any number of optimisation algorithms could be iteratively used to improve the design parameters (rod directions). For the reasons discussed in the Introduction we use a MOGA; details are given in Section 5. A key benefit of the scheme described in this paper is that it allows exploration of a wide variety of different grid designs without the need to recalculate and update complex free-form geometry. Instead we alter (anisotropic) material stiffness matrices within a continuum model.

Upon completion of the optimisation process optimal designs are defined in terms of continuum shells with given anisotropic material properties. Section 6 describes how these results can be used to synthesise exact structural layouts.

3 Homogenization

3.1 Overview

The algorithm described in this paper is based upon the lattice of rods being represented by an anisotropic continuum material of equivalent stiffness. The optimization can therefore be applied to any structure consisting of a repeating quadrilateral unit cell, such as a triangulated single layer grid (see Figs. 1 and 3a), a quadrilateral single layer grid or a double layer space frame. A novel aspect of the approach used in this paper is that we consider a variable geometry for the unit cell. So for the triangulated unit cell shown in Fig. 3b the angle α is a variable. Therefore a scheme is required to find the stiffness matrix for this homogenised plate, as a function of the geometrical parameters α and β. This matrix will give the stress resultants $(N_x, N_y, N_{xy})^T$ and bending / twisting moments per unit length $(M_x, M_y, M_{xy})^T$ in terms of mid-plane strains $(\varepsilon_x^0, \varepsilon_y^0, \varepsilon_{xy}^0)^T$ and curvatures $(\kappa_x, \kappa_y, \kappa_{xy})^T$ for the homogenised plate:

$$\begin{bmatrix} N_{xx} \\ N_{yy} \\ N_{xy} \\ M_{xx} \\ M_{yy} \\ M_{xy} \end{bmatrix} = \begin{bmatrix} A_{11} & A_{12} & A_{16} & B_{11} & B_{12} & B_{16} \\ A_{21} & A_{22} & A_{26} & B_{21} & B_{22} & B_{26} \\ A_{61} & A_{62} & A_{66} & B_{61} & B_{62} & B_{66} \\ B_{11} & B_{12} & B_{16} & D_{11} & D_{12} & D_{16} \\ B_{21} & B_{22} & B_{26} & D_{21} & D_{22} & D_{26} \\ B_{61} & B_{62} & B_{66} & D_{61} & D_{62} & D_{66} \end{bmatrix} \begin{bmatrix} \varepsilon_x^0 \\ \varepsilon_y^0 \\ \varepsilon_{xy}^0 \\ \kappa_x \\ \kappa_y \\ \kappa_{xy} \end{bmatrix} \quad (1)$$

This approach can be viewed as a subset of free material optimization (Bendsoe and Sigmund 2003). In the free material approach components of the stiffness matrix are individually optimized (subject to some overall constraints, such as positive definiteness), and then a post processing step attempts to fit a real material/structure to the optimised stiffness matrix. In our approach the stiffness matrix is formulated from the desired unit cell, which reduces the design space but eliminates the need for post processing.

3.2 Derivation

The homogenized stiffness matrix is found by calculating the stiffness of a grid unit cell (Fig. 3), which is subjected to periodic boundary conditions and Kirchhoff's thin plate assumption. Hence the kinematic variables for the plate are mid-plane strains and out of plane curvatures:

$$\varepsilon_x = \frac{\partial u}{\partial x} \tag{2}$$

$$\varepsilon_y = \frac{\partial v}{\partial y} \tag{3}$$

$$\varepsilon_{xy} = \frac{\partial u}{\partial x} + \frac{\partial v}{\partial y} \tag{4}$$

$$\kappa_x = -\frac{\partial^2 w}{\partial x^2} \tag{5}$$

$$\kappa_y = -\frac{\partial^2 w}{\partial y^2} \tag{6}$$

$$\kappa_{xy} = -2\frac{\partial^2 w}{\partial x \partial y} \tag{7}$$

The periodic boundary condition procedure described by Kueh and Pellegrino (2007) is followed, to calculate the coefficients of the ABD matrix (1) (c.f. classical laminate plate theory of composites). Opposing pairs of boundary nodes on the unit cell are considered (e.g. a and c, b and f) in Fig. 4. We couple their displacements and rotations by integrating (2–7) between limits defined by these pairs of nodes:

$$u^j - u^i = \varepsilon_x \Delta l_x \tag{8}$$

$$v^j - v^i = \frac{1}{2}\varepsilon_{xy} \Delta l_x \tag{9}$$

$$u^l - u^k = \frac{1}{2}\varepsilon_{xy} \Delta l_y \tag{10}$$

$$v^l - v^k = \varepsilon_y \Delta l_y \tag{11}$$

$$\theta_x^j - \theta_x^i = -\frac{1}{2}\kappa_{xy} \Delta l_x \tag{12}$$

$$\theta_y^j - \theta_y^i = \kappa_x \Delta l_x \tag{13}$$

$$\theta_x^l - \theta_x^k = -\kappa_y \Delta l_y \tag{14}$$

$$\theta_y^l - \theta_y^k = \frac{1}{2}\kappa_{xy} \Delta l_y \tag{15}$$

$$\theta_z^j - \theta_z^i = 0 \tag{16}$$

$$\theta_z^l - \theta_z^k = 0 \tag{17}$$

where superscripts i, j and k, l describe pairs of opposing nodes, as per Tables 1 and 2.

The grid geometry is assumed to be planar, as shown in Fig. 4. Therefore even before the numerics are implemented it is clear that there can be no coupling between stretching and bending effects, i.e. $B_{nm} = 0$, due to symmetry. In addition $A_{16} = A_{26} = D_{16} = D_{26} = 0$ (c.f. balanced symmetric lay-up in laminated plates). This may not be true in all practicable grid structures, however the general homogenisation technique described in this section is always applicable.

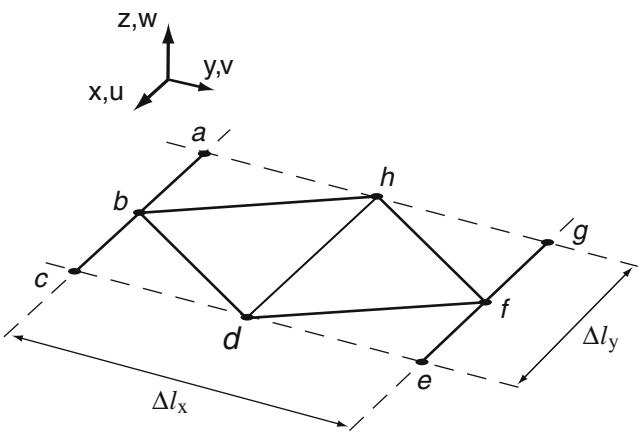

Fig. 4 Unit cell definition, as used in periodic boundary conditions equations

Table 1 Nodal pairs for x-direction periodic boundary conditions

Superscripts	i	j
Nodal pair 1	a	c
Nodal pair 2	h	d
Nodal pair 3	g	e

Table 2 Nodal pairs for y-direction periodic boundary conditions

Superscripts	k	l
Nodal pair 1	a	g
Nodal pair 2	b	f
Nodal pair 3	c	e

The remaining stiffness matrix coefficients are found by carrying out six separate finite element analyses. For each analysis we calculate the nodal reactions due to a unit deformation imposed on the unit cell, as shown in Table 3.

Virtual work is then used to calculate the matrix components A_{11} to D_{66} in (1). For example:

$$M_{xx}\kappa_y \Delta l_x \Delta l_y = \sum_{nodes} \left(F_x u + F_y v + F_z w + M_x \theta_x + M_y \theta_y + M_z \theta_z\right) \tag{18}$$

where F_x, F_y, F_z, M_x, M_y, M_z are nodal reactions from analysis 4 (corresponding to M_{xx}, the 'real' set), whilst $u, v, w, \theta_x, \theta_y, \theta_z$ are nodal displacements/rotations from analysis 5 (corresponding to κ_y, the 'virtual' set). For this example $\kappa_y = 1$ so from Eq. 1 $M_{xx} = D_{12} = [ABD]_{45}$. Therefore:

$$D_{12} = [ABD]_{45} = \frac{\sum_{nodes} \left(F_x^4 u^5 + F_y^4 v^5 + F_z^4 w^5 + M_x^4 \theta_x^5 + M_y^4 \theta_y^5 + M_z^4 \theta_z^5\right)}{\Delta l_x \Delta l_y} \tag{19}$$

or more generally

$$[ABD]_{ij} = \frac{\sum_{nodes} \left(F_x^i u^j + F_y^i v^j + F_z^i w^j + M_x^i \theta_x^j + M_y^i \theta_y^j + M_z^i \theta_z^j\right)}{\Delta l_x \Delta l_y} \tag{20}$$

for i = 1,2,3,4,5,6 and j = 1,2,3,4,5,6.

Table 3 Applied deformations

Analysis number	ε_x	ε_y	ε_{xy}	κ_x	κ_y	κ_{xy}
1	1	0	0	0	0	0
2	0	1	0	0	0	0
3	0	0	1	0	0	0
4	0	0	0	1	0	0
5	0	0	0	0	1	0
6	0	0	0	0	0	1

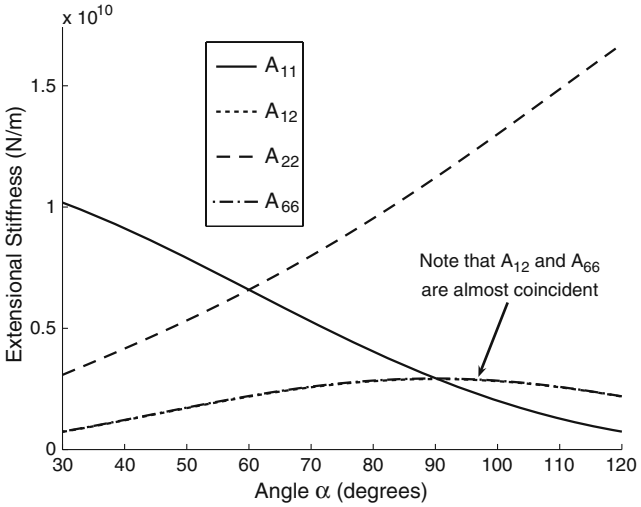

Fig. 5 Extensional stiffness matrix coefficients

For the purposes of this paper the unit cell geometry is variable (due to angle α), hence the ABD matrix must be calculated for a wide range of values of α. ABD matrix coefficients for the unit cell in Fig. 3b are plotted against α in Figs. 5 and 6. Rod properties are as follows: $I_{xx} = 0.88$ m^4, $I_{yy} = 0.0072$ m^4, $J = 0.015$ m^4, $A = 0.14$ m^2 and $L = 5$ m, which correspond to the grid in Example 1 (Section 8).

For simple unit cells it is possible to derive the ABD matrix analytically, as function of α. For example, the authors give the analytical expressions for a parallelogram unit cell (Fig. 3b without the vertical rods) in Winslow (2006). However, arguably one of the

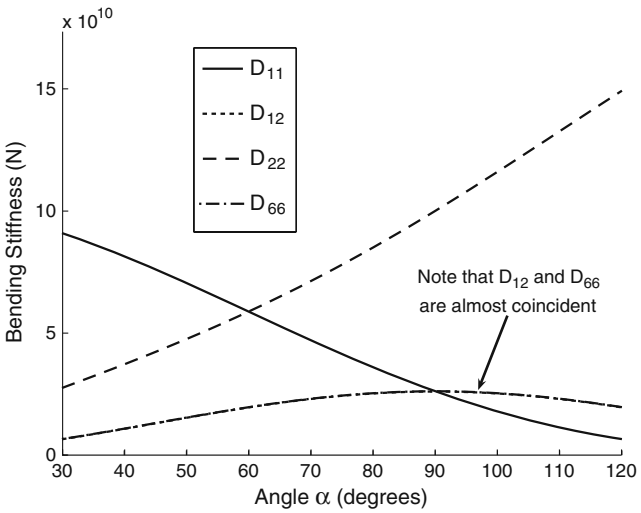

Fig. 6 Bending stiffness matrix coefficients

biggest strengths of the research presented in this paper is that the homogenization process allows us to readily consider optimization of structures with any unit cell, however complex. Thus analytical derivations would not always be practical, and so homogenization by the periodic boundary conditions approach is generally preferred.

3.3 Validation

Validation is required in order to show that the homogenised approach can be used to model the behaviour of a discrete grid shell to a reasonable degree of accuracy. Absolute precision is not mandatory, since the purpose is not to carry out detailed design checks. Instead the aim is to develop a tool which facilitates exploration of a wide range of designs using stiffness properties which are indicative of the final discrete grid structure.

The homogenised approach is validated by consideration of a piece of discrete structure consisting of N unit cells side by side, see Fig. 7. In this paper each rod in the structure is meshed with beam elements for FE analysis, though validation could also be conducted experimentally (Aoki and Yoshida 2007). For example, to ascertain the accuracy of the homogenised bending stiffness a positive couple is applied to the top edge of the structure and a negative couple is applied to the bottom edge. Stiffness is then calculated from the resulting edge rotations, which are dependent upon the width of the validation model. Figure 8a and b show stiffness versus width for A_{11} and D_{22} validation tests (tests were carried out for all other ABD matrix entries, but are not shown here for conciseness). For small N it can be seen that end effects significantly reduce the stiffness of the validation model. The y-intercept of the best fit line gives stiffness of the discrete validation model without end effects (as width tends to infinity). Any discrepancy between the y-intercept and the homogenized stiffness value (previously calculated by periodic boundary conditions and shown in Figs. 5 and 6) would indicate inaccuracies in the homogenized approach, e.g. because it cannot capture in-plane rotations. However, the discrepancy was approximately 0.1% for all entries in the ABD matrix, and is in fact not visible in Fig. 8a and b; an adequately small source of error.

The validation charts Fig. 8a and b serve another purpose; they can give an indication of the circumstances in which the homogenized ABD matrix can be successfully used to model a complete grid shell. For instance, suppose we wish to synthesize a grid with rod spacing $L = 0.5$ m. If curvature and stress variations are small over a length scale of around 3–4 m then $N \approx 7$,

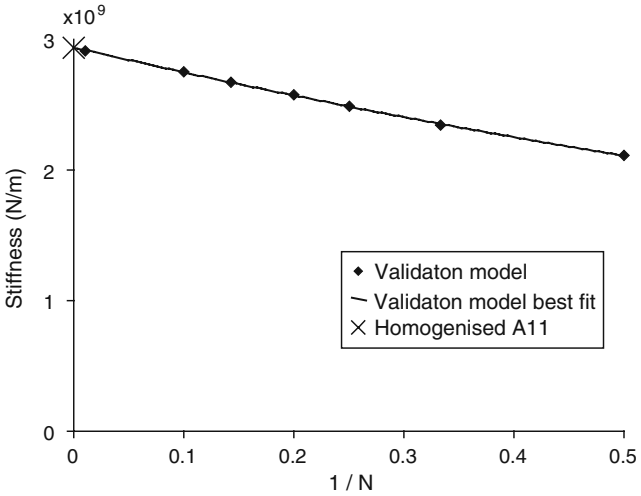

(a) A 11 validation

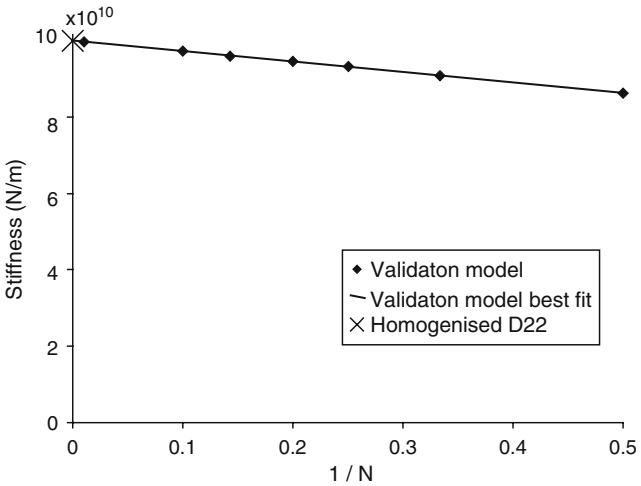

(b) D22 validation

Fig. 8 Comparison of homogenised stiffness with the variable width discrete validation model shown in Fig. 7. (N = number of unit cells in model) (**a**, **b**)

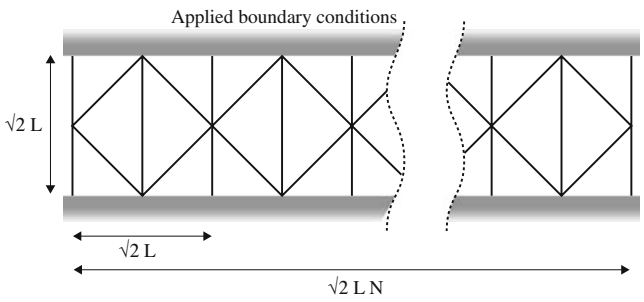

Fig. 7 Variable width discrete analysis model. N = number of unit cells under consideration

and so Fig. 8a and b indicate that errors of order 5% are to be expected. However, if curvature and stress vary over a much shorter length scale then N drops, and expected errors will rise. A smaller value of rod spacing L would then be required in order to keep errors to an acceptable level.

4 Solution representation

In order to optimize the homogenized structure one could assign two independent design variables to every shell element in the FE mesh (angle between the rods α, and rotation of the principal material directions β). However, from a practical point of view this is unnecessary; we hope to obtain structures with some degree of rod continuity and with limited curvature, so that it is both constructible and visually appealing. Therefore the designer chooses a number of points on the surface Ω at which α and β are independently defined, see Fig. 9. Piece-wise linear interpolations are then used to define α and β at the centroid of every finite element between these 'design points'. So, for instance, if the surface Ω was meshed with shell elements, any element centroid lying within the gray shaded region would be assigned rod angles based on a linear interpolation of α_2,α_4,α_7 and β_2,β_4,β_7 . The interpolation patches can be created manually or by Delaunay triangulation of the 'design' points in the surface parameter domain. Note that quadratic interpolation patches could be used if mid-side design points were defined; it is simply a subclass of the same problem.

Given that the surface Ω may by highly curved, it is necessary that the rod angles are defined relative to local coordinate systems (the direction of which must vary smoothly over the surface). In this paper all surfaces are represented using NURBS, thus they have an underlying (u, v) parametrization. At any point on the surface we can therefore define rod angles to be measured clockwise from the positive u-direction, as shown in Fig. 10. For surfaces with complex topology each region becomes a chart with its own (u, v) parametrization, and transition functions ensure continuity between charts (as is well established in field of discrete differential geometry (Tong et al. 2006)).

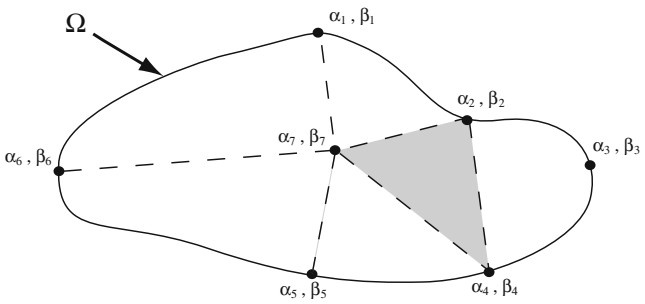

Fig. 9 Subdivision of surface Ω into regions using 7 points

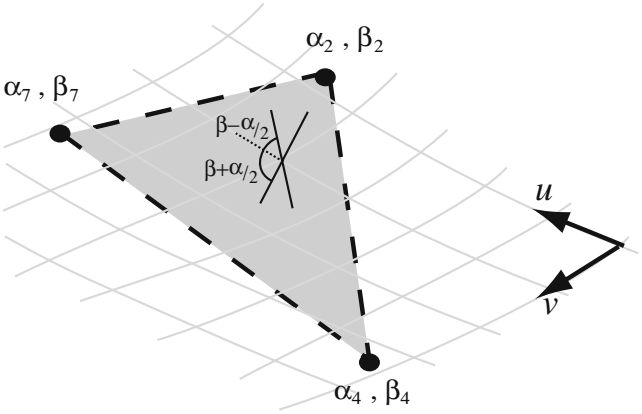

Fig. 10 Single region (from Fig. 3), shown with underlying (u,v) surface parametrization. Angles of the two sets of rods, $\beta + \alpha/2$ and $\beta - \alpha/2$, are measured anti-clockwise from local u-axis (*dotted line*)

The above procedure ensures that there is tangent continuity of the rods between the interpolation patch region. However, it relies upon having a surface parameterization with low distortion of angles and lengths. For some surface geometries it is possible to obtain a satisfactory surface parameterization from commercially available CAD packages. Creation of low distortion surface parameterizations for any given surface has been addressed in the field of computer graphics e.g. Computational Geometry Algorithms Library (Saboret et al. 2007).

Although commonly used in genetic algorithms, a bit string solution encoding is not used here for a number of reasons:

- Use of real numbers allows continuous variables to be represented exactly.
- Simulated binary crossover (Deb 2001) allows real-numbered representations to be successfully evolved.
- A one dimensional bit string would result in loss of the (two dimensional) surface geometry and regional connectivity information when considering crossover and mutation operators.

The data used to represent each solution is therefore real numbered values of α_i and β_i for all region corner nodes.

5 Optimization scheme

The flow chart in Fig. 11 shows the multi-objective optimization procedure. The aim is to minimize a number of objectives

$$f_1(\boldsymbol{\alpha}, \boldsymbol{\beta}),\ f_2(\boldsymbol{\alpha}, \boldsymbol{\beta}) \ldots\ldots f_n(\boldsymbol{\alpha}, \boldsymbol{\beta}) \tag{21}$$

subject to

$$(0 + \sigma) < \alpha_i < (180 - \sigma) \tag{22}$$

$$0 < \beta_i < 180 \tag{23}$$

where:

σ = minimum allowable angle between the rods, and

i = design point number

The flowchart is explained in more detail by the subsections below.

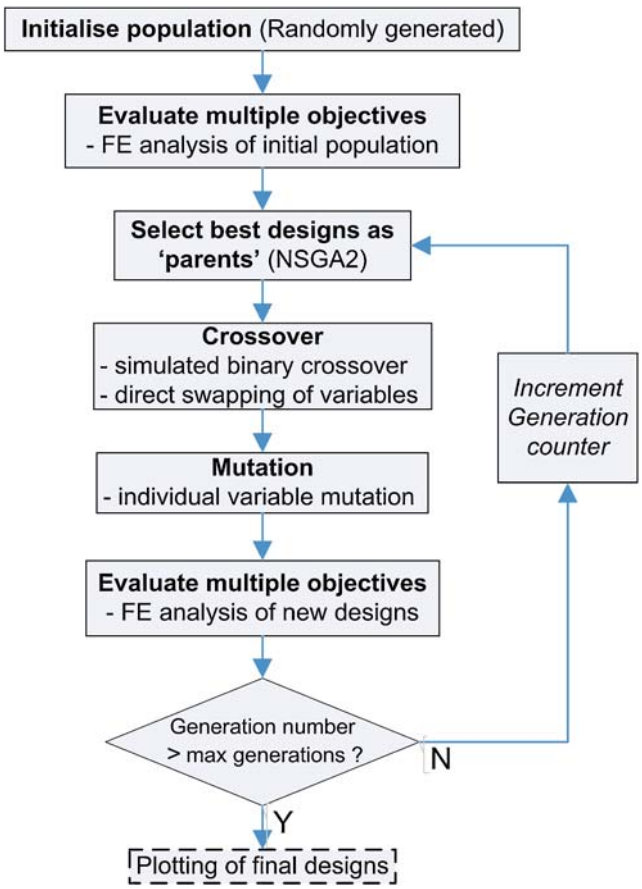

Fig. 11 Multi-objective optimization procedure

5.1 Selection

A key part of the optimization process is selection of suitable parents from which the next generation of designs will be evolved. For this purpose an elitist algorithm, the Non-dominated Sorting Genetic Algorithm II (NSGA-II) (Deb et al. 2000), is used since it has been shown that for most multi-objective test problems elitist algorithms perform better than other selection methods. NSGA-II chooses parents using not only their fitness but also by considering their spread. Thus a more diverse Pareto-optimal front is generated and so there is greater freedom when choosing a design from the final population. The PISA implementation of NSGA-II (Bleuler et al. 2003) is used for this paper.

5.2 Crossover operators

For this paper two specific operations are used to create new designs from a pair of parents:

1. Simulated binary crossover (SBX)
   A real-valued representation of designs is used, so standard bit string one point cross-over operators are not applicable. However, simulated binary cross-over (Deb 2001) overcomes this limitation whilst allows retention of the other benefits associated with a real valued representation.
2. Uniform crossover
   Direct swapping of a design variable between two parents (c.f. two-point bit-string crossover)

5.3 Mutation operators

A mutation operator is used which considers each real-numbered design variable in turn. A random number is generated and if it is less than the pre-specified mutation probability then that design variable is mutated. A non-uniform probability density function is used so that small changes in the design variable have a high likelihood of occurrence, whilst larger mutations are rare.

6 Visualization of results

The output of the main optimization loop is a population of designs, and for each design α and β are defined everywhere on the surface (see Section 5). The local coordinate systems (from which these angles are measured) are known, hence it is a trivial matter to create a pair of vector fields on the surface which define the directions of the two primary sets of rods. Note

that these directions are defined by angles $\beta + \alpha/2$ and $\beta - \alpha/2$, see Fig. 10.

Representing the results is a post-processing step, and two alternative methods are proposed:

1. Conduct a minimal amount of post-processing; simply draw the directions of these vector fields at a number of discrete points on the surface e.g. at the centre of each region. The designer would then use these optimized directions as guidance whilst drawing a complete grid, over which they have ultimate control.
2. Synthesize a complete grid, by plotting two sets of rod paths which follow the two optimized vector fields.

A simple step-wise algorithm is used for the rod path plotting in this paper. The user picks a start point (which may be the top of a column, apex of a dome or a point on the surface boundary), and a path is drawn from that point in a step-wise manner such that it is tangential to one of the vector fields everywhere along its length (c.f. plotting streamlines in fluid flow). This process is repeated until the desired density of rods is achieved for both vector fields. For a triangulated grid, the two primary directions are drawn first and triangulation is added afterwards. Research into the application of automated global rod plotting algorithms (such as Michalatos and Kaijima (2007) and Tong et al. (2006)) is currently ongoing; more detail is given in Winslow et al. (2008).

7 Example I

The first illustrative example is a dome subject to two eccentric load cases. The surface is a spherical cap with a height of 25 m, cut from a sphere of radius 174.5 m (cap diameter is 180 m), see Fig. 12a. Also shown in this figure are three support points which are fixed against translation, and the surface is shaded according to the wind load objective (see below). The objectives are:

1. Minimize deflection under combined self-weight and asymmetric wind loading. Referring to Fig. 12a the dark grey area (upwind 1/3 of the surface) is subject to +2 kPa, light gray area (downwind 2/3 of surface) is subject to −1 kPa).
2. Minimize deflection under combined self-weight and 2 m/s^2 lateral acceleration (indicative of the peak acceleration in an earthquake)

The structure is to be constructed from a triangulated grid of rods (see Fig. 12b) with perpendicular spacing $L = 5$ m. However, given the large span of this

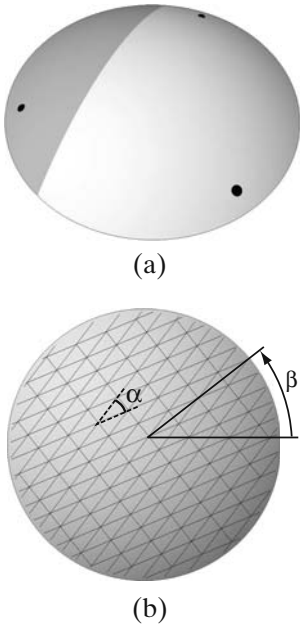

Fig. 12 Spherical cap problem definition. **a** Support points shown in *black*, and wind loading zones by *gray shading*. **b** Schematic definition of rod angles

dome each 'rod' is a 5 m deep planar truss made from 0.5 m diameter steel tubes of wall thickness 0.05 m. It is straightforward to implement this more complex structure because the homogenized stiffness matrix is simply calculated using values of I_{xx}, I_{yy}, J, A which are representative of a truss rather than of a single tube.

For simplicity in this preliminary example each grid design is represented by two design variables

$$10 < \alpha < 170 \quad \text{and} \quad 0 < \beta < 180$$

as shown in Fig. 12b. Thus design space is represented by a pair of contour plots:

Wind loading objective = F(α,β) in Fig. 13
Earthquake objective = F(α,β) in Fig. 14

These contour plots are created numerically by evaluating the objective functions for many different values of α and β. This allows us to readily visualize the progress of the genetic algorithm. Starting with an initial population of 20 random designs, the evolving population is plotted at generation numbers 1,5 and 20 on a trade-off plot (Fig. 15) and on the two contour plots (Figs. 13 and 14). Note that the scale on Fig. 15 is enlarged, thus many designs in generation 1 are not visible.

Also included on the trade-off plot (Fig. 15) is the optimal Pareto-front. This has been calculated numerically from the two contour plots, and gives a effective visual indication of how rapidly the genetic algorithm is converging towards the optimum. A commonly used measure of convergence is the mean Euclidean distance between all designs in a given generation and the

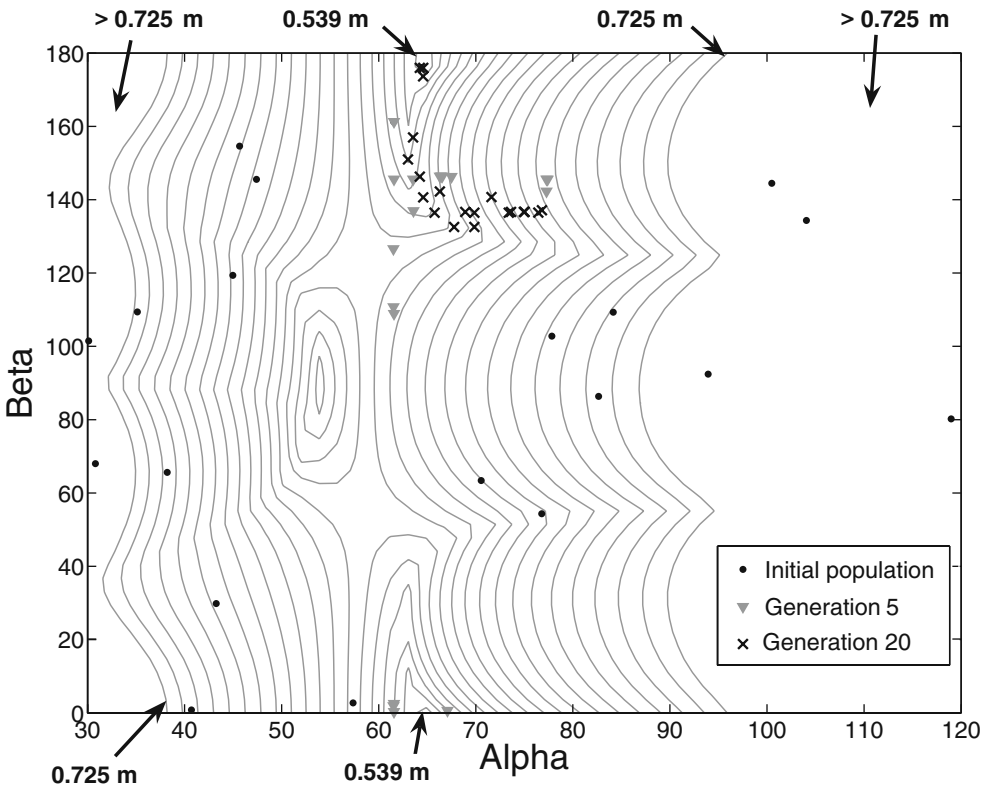

Fig. 13 Contour plot of objective 1 (deflection due to wind) with genetic algorithm results

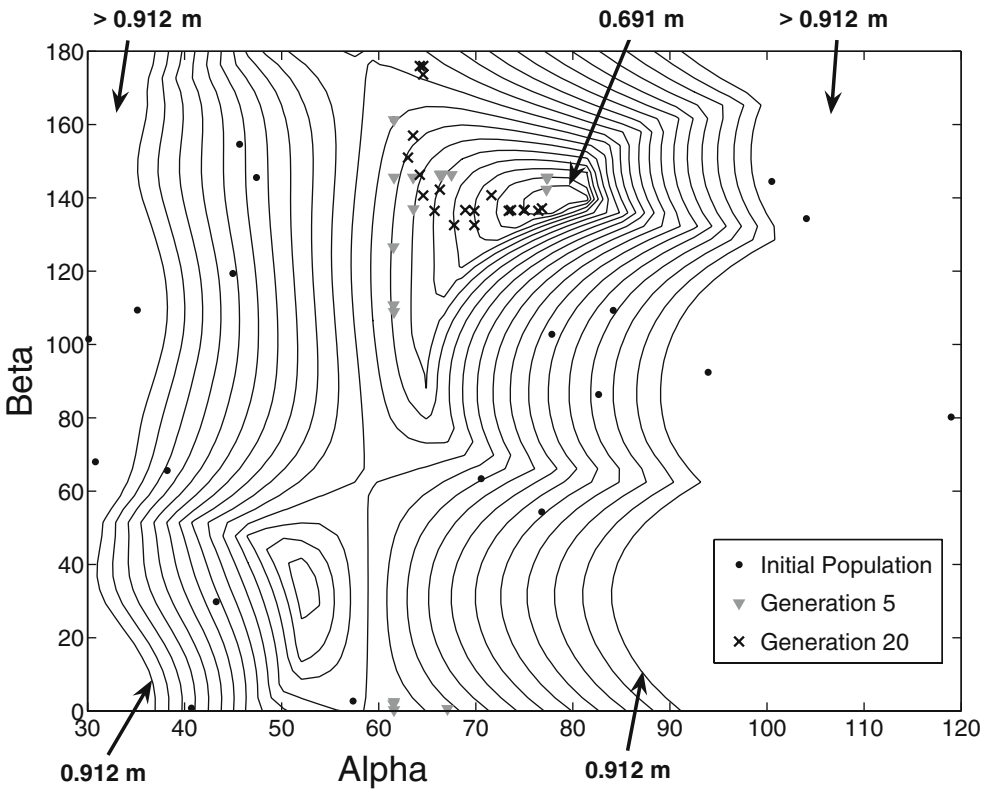

Fig. 14 Contour plot of objective 2 (earthquake deflection) with genetic algorithm results

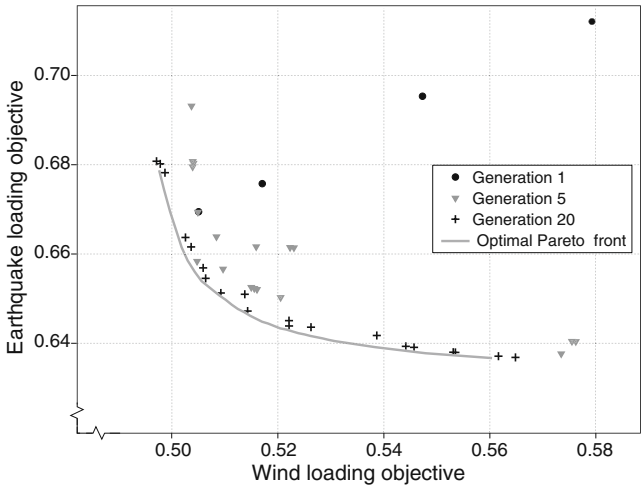

Fig. 15 Trade-off plot for generations 1, 5, 20, and optimal Pareto-front

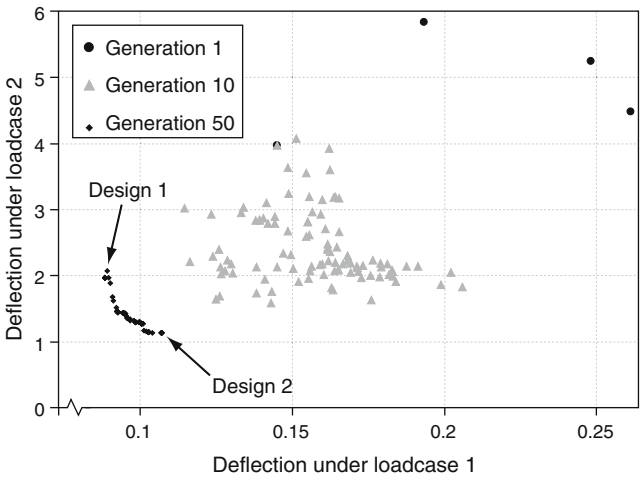

Fig. 18 Trade-off plot showing design evolution over 50 generations

Fig. 16 Example II problem definition. **a** Doubly curved surface geometry, with end supports shown in *black* **b** Surface subdivision scheme (6 design points, 4 regions)

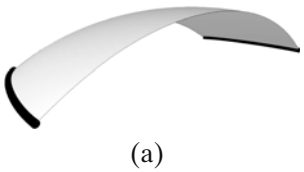

(a)

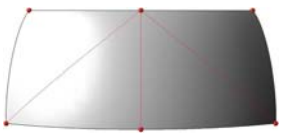

(b)

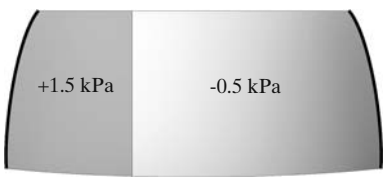

(a) Asymmetrical wind loading

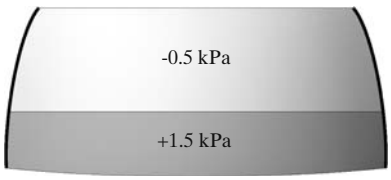

(b) Symmetrical wind loading

Fig. 17 Wind loading definition for example problem II (**a**, **b**)

optimal Pareto-front (Deb 2001). For this example the convergence is very rapid; after just 20 generations the mean Euclidean distance is 7.4×10^{-4} (which is $\approx 0.1\%$ of the value of the objective functions).

It is interesting to note that in Fig. 13 a number of the designs in the 20th generation have converged to a minima where the value of β is very near its upper limit of 180 degrees, whereas the maximum value of β in the initial population is ≈ 160. It was thus found that a

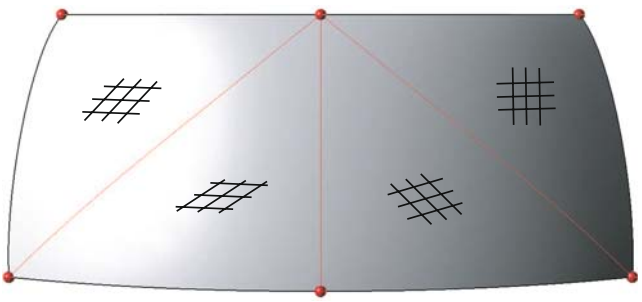

(a) Optimal directions

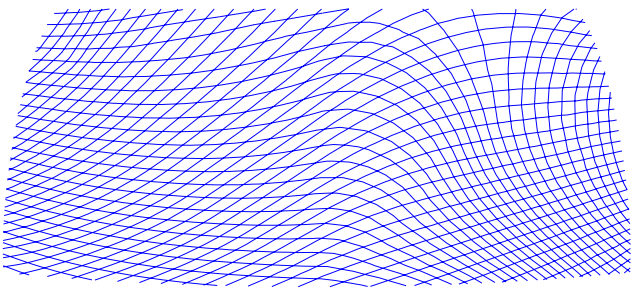

(b) Complete grid

Fig. 19 1st design from 50th generation: High stiffness for load case 1 (**a**, **b**)

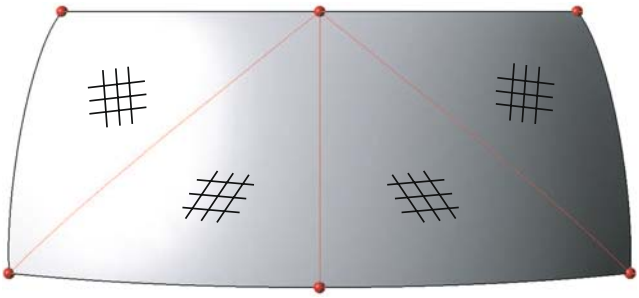

(a) Directions

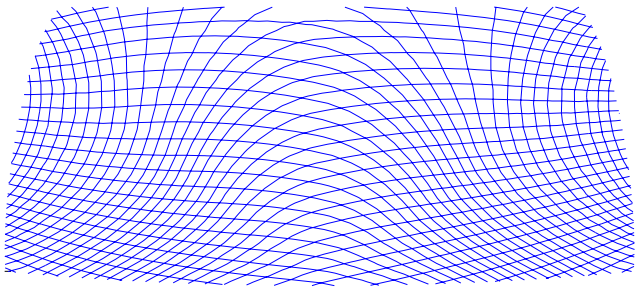

(b) Complete grid

Fig. 20 2nd design from 50th generation: high stiffness for load case 2 (**a**, **b**)

relatively large amount of mutation was crucial in order to successfully explore the design space and converge to a minima near the limits of design variables. A study was carried out to investigate the effect of the genetic algorithm parameters on the rate of convergence. Using the mean and standard deviation of the Euclidean distance (as described above), the following probabilities were found to give good convergence: SBX = 0.6, Variable swap = 0.2 and Non-uniform mutation = 0.2.

8 Example II

For the second example a 54 m span doubly-curved arch will be considered. The surface, shown in Fig. 16a, is fixed against translation at both ends. The grid structure will be constructed from a bi-directional grid of steel tubes with aluminium infill panels. The steel tubes are 114.3 mm in diameter and have 5 mm wall thickness. The panels are 2 mm thick, and it is assumed that they are rigidly attached to the bi-directional grid. The perpendicular spacing between the rods is taken as 0.5 m, which means that the total length of rods in the structure is fixed. Therefore total structural mass is constant throughout the optimization. Two objective functions are considered:

1. Minimize deflection under combined self-weight and asymmetrical wind loading from the prevailing direction (see Fig. 17a)
2. Minimize deflection under combined self-weight and symmetrical wind loading from direction 2 (see Fig. 17b)

The surface is divided into a number of regions; 6 design points are chosen for this example, giving 4 regions and 12 design variables (see Fig. 16b). A population size of 100 is used, and the initial population is generated randomly.

The results from 50 generations of evolution are shown in Fig. 18. It should be noted that only some of the designs from the initial population can be seen on this chart, since the others are off the scale. By the 50th generation a very clear trade-off surface of optimal designs has evolved, and two of these are plotted in Figs. 19b and 20b. A rendered image of Design 2 is

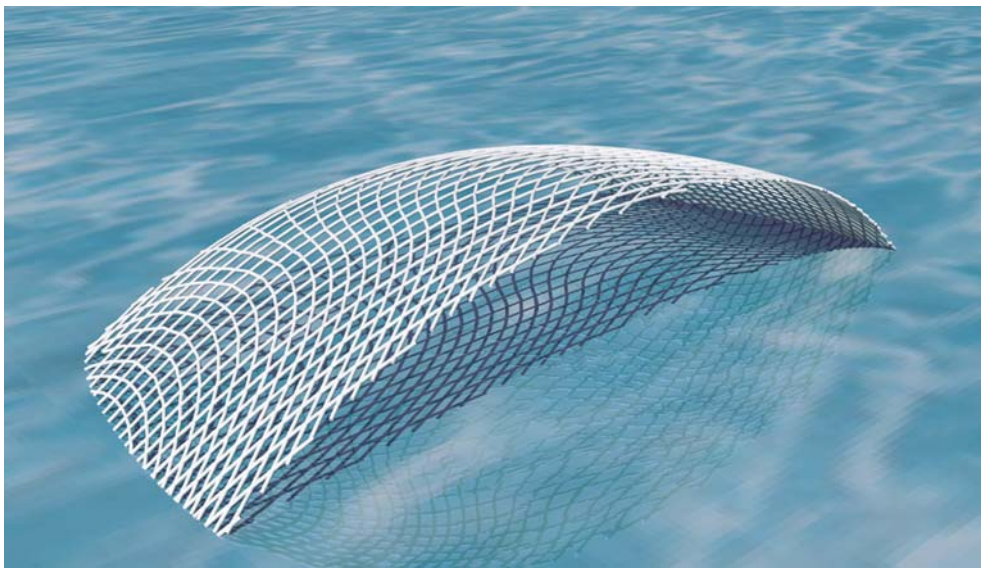

Fig. 21 Design 2, from 50th generation, has high resistance to loadcase 1 (symmetrical wind loading)

shown in Fig. 21. Visual inspection of these diagrams shows that the latter design (which is optimal for the symmetric wind load case) is very close to being symmetrical; the mean difference between rod angles at one region corner node and the opposing corner node is ∼5 degrees. Hence despite not enforcing symmetry (e.g. by only considering half of the structure) the genetic algorithm has converged to a logical, rational solution. The small amount asymmetry in Fig. 20b could be reduced further by adopting a self-adaption approach (more akin to Evolution Strategies) whereby the probability and magnitude of any mutations is reduced in later generations, hence increasing the ability to converge to the optimum.

9 Conclusions and further work

A novel tool for multi-objective optimization of grid structures has been presented in this paper. Given a surface and a desired grid type it has been shown, by example, that the rod orientations can be successfully evolved to create a population of optimal designs. The homogenization process allows us to synthesize any type of grid structure provided it has a repeating unit cell e.g. triangular, double-layer or quadrilateral with infill panels etc. The sample problems presented in this paper suggest that using a relatively modest number of generations it is possible to evolve a diverse range of solutions, which appear constructible and visually rational.

The main direction of future research is to develop a reliable automated scheme for plotting optimized rod paths. It is envisaged that this will form part of a second-pass optimization and refinement tool, in which the objective functions are evaluated by FE analysis of the discrete grid of beams/rods. It may also be interesting to compare results from multi-objective optimization to analytical solutions e.g. Rozvany and Prager (1979).

Acknowledgements We would like to acknowledge the financial support of the UK Engineering and Physical Sciences Research Council and of Buro Happold.

References

Aoki T, Yoshida K (2007) Feasibility study of triaxially-woven fabric composite for deployable structures. In: 48th AIAA/ASME/ASCE/AHS/ASC structures, structural dynamics, and materials conference, Waikiki, April 2007

Bendsoe MP, Sigmund O (2003) Topology optimization: theory, methods and applications. Springer, Berlin Heidelberg New York

Bleuler S et al (2003) PISA—a platform and programming language independent interface for search algorithms. In: Conference on evolutionary multi-criterion optimization, Faro, 8–11 April 2003

Deb K (2001) Multi-objective optimization using evolutionary algorithms. Wiley, New York

Deb K et al (2000) A fast elitist non-dominated sorting objective genetic algorithm for multi-objective optimization: NSGA-II In: Proceedings of the parallel problem solving from nature VI (PPSN-VI), Paris, September 2000

Gurdal Z, Olmedo R (1993) In-plane response of laminates with spatially varying fiber orientations. Variable stiffness concept. AIAA J 31:751–758

Kueh ABH, Pellegrino S (2007) ABD matrix of single-ply triaxial weave fabric composites. In: 48th AIAA/ASME/ASCE/AHS/ASC structures, structural dynamics, and materials conference, Waikiki, April 2007

Maute M, Ramm E (1997) Adaptive topology optimization of shell structures. AIAA J 35(11):1767–1773

Michalatos P, Kaijima S (2007) Design in a non homogeneous and anisotropic space. In: International association of shell and spatial structures symposium, Venice, 3–6 December 2007

Rozvany GIN, Prager W (1979) A new class of optimization problems: optimal archgrids. Comput Methods Appl Mech Eng 19:127–150

Rozvany GIN, Wang CM, Dow M (1982) Archgrids and cable networks of optimal layout. Comput Methods Appl Mech Eng 31:91–113

Saboret L, Alliez P, Lévy B (2007) CGAL user and reference manual: planar parameterization of triangulated surface meshes. CGAL Editorial Board

Schlaich J, Schober H, Kurschner K (2005) New trade fair in Milan—grid topology and structural behaviour of a free-formed glass-covered surface. Int J Space Struct 20:1–14

Tong Y, Alliez P, Cohen-Steiner D, Desbrun M (2006) Designing quadrangulations with discrete harmonic forms. In: SGP '06: proceedings of the fourth eurographics symposium on geometry processing, Cagliari, 26–28 June 2006, pp 201–210

Winslow P (2006) Free-form grid structures. Internal Report, Cambridge University Engineering Department

Winslow P, Pellegrino S, Sharma SB (2007) Mapping two-way grids onto free-form surfaces. In: International association of shell and spatial structures symposium, Venice, 3–6 December 2007

Winslow P, Pellegrino S, Sharma SB (2008) Subdivision techniques for optimization of free-form structures. In: International association of shell and spatial structures symposium, Acapulco, 27–31 October 2008